An introduction to Eulerian Geometrical Optics (1992-2002)

Jean-David Benamou

INSTITUT NATIONAL DE RECHERCHE EN INFORMATIQUE ET EN AUTOMATIQUE

An introduction to Eulerian Geometrical Optics (1992-2002)

J.-D. Benamou

N° 4628

novembre 2002

THÈME 4

Rapport de recherche

INRIA
ROCQUENCOURT

An introduction to Eulerian Geometrical Optics (1992-2002)

J.-D. Benamou

Abstract: This document is an attempt at introducing the different "Eulerian" numerical methods which have recently been developed for the simulation of geometric optics and related models

Key-words: Hamilton-Jacobi, Caustic, Hamiltonian System, Ray Tracing, Viscosity Solution, Level Set method, Wave equation, Kinetic equation, Upwind Solvers, Geometrical Optics

Une introduction à l'optique géométrique Eulérienne (1992-2002)

Résumé : Ce document essaye de présenter de manière exhaustive les différentes méthodes Eulériennes récemment dévelopées en vue de la simulation de l'optique géom'etrique et de phénomènes associés.

Contents

Dedicated to S. Osher on his 60th birthday.

Introduction

I arrived at UCLA in the fall of 1992. At that time a post-doc, I had two papers on my desk. The first one, *"Upwind Finite-Difference Calculation of Travel-Times", Geophysics , 56:812–821, 1991* by J. Van Trier and W. W. Symes was carrying two messages :

1. as claimed by J. Vidale [81], a geophysicist, the Eikonal equation can be solved as partial differential equation (PDE) using a finite-difference solver sharing the upwind properties of schemes used for hyperbolic problems.

2. The second message, more subtle, is the observation that the obtained solution is not equivalent to the classical output of the traditional numerical ray tracing (RT) method. It was conjectured that only a part of the ray tracing solution is obtained using a direct resolution of the Eikonal equation and corresponds in the Geophysical terminology to the "first arrival travel-times".

Message #1 seemed to pave the way to a new field of geophysical application for the applied mathematicians working on hyperbolic problems. Indeed, the Eikonal equation was already used as a prototype in the mathematical theory of viscosity solution of Hamilton-Jacobi (HJ) equation [31] and their numerical analysis (see for instance [32] [77]). ENO (Essentailly Non Oscillatory) solvers, for instance, had their HJ version [69]. Message #2 however was bad news. Some analysis was clearly needed to understand the precise relation between the viscosity "first arrival" single-valued solution and the full GO (Geometrics Optics) solution potentially multi-valued. Moreover there was no indication that any HJ solver would be able to compute the GO solution and, in that case, would be of limited use as later arrivals are absolutely needed (see [26]) in many geophysical applications such as migration ([18] [79] [19]) for instance.

An answer came almost instantly in the form of the second paper, a preprint when I was studying it in 1992 : *"Numerical resolution of the high frequency asymptotic expansion of the scalar wave equation", J. Comp. Physics, 120:145–155, 1995* by B. Engquist, E. Fatemi and S. Osher (instant reply is a typical Osher feature). They proposed an inventive procedure to extend the Eikonal finite difference solution when it becomes multi-valued. As we will see, this algorithm was incomplete but it was the start of a new field of research we will refer to as Eulerian GO.

Eulerian GO has maintain a high level of activity and interest in the applied mathematics community in general and in the "level set" community in particular. The reason is, the Eikonal equation lies at the crossroad of many different scientific fields : It is the high frequency approximation of different types of wave equation [35] [30] but can also be derived using the calculus of variations and Fermat's principle [42] [84]. The same asymptotic method, called WKB, is also used for the Schrödinger equation and there has recently been some interest in the application of semi-classical limits [61] to the Hemlholtz equation [16] [25] [43], the equation in the high frequency limit is a "Liouville" kinetic equation. The

failure of GO to represent accurately the wave-field near caustics or when diffraction occurs has kept busy several generations of mathematicians [39] [21] [17] and is closely linked to the possible multi-valuedness of GO solutions. The Hamiltonian structure of the problem has been extensively studied in differential simplectic geometry [33] [49] [7] which is the fundamental tool to understand the qualitative structure of GO solutions. It is also a tool in the application of microlocal analysis to the controllability of the wave equation [8]. Viscosity solutions have ground in optimal control theory (see [9] for a review) while numerical upwind schemes are traditionally used to solve hyperbolic conservations laws [44]. Finally, and this is probably why Stan Osher has pioneered the field, the idea of replacing RT, i.e solving ordinary differential equations (ODEs) for Lagrangian trajectories and other associated Lagrangian variables, with the computation of Eulerian variables, solution of PDEs, is at the heart of the "level set" method [68]. Basically, the "level set" method keeps track of the Lagrangian trajectories using (precisely) the level sets of the associated Eulerian variable. This variable is the solution of a PDE usually computed on a finite difference grid. In Eulerian GO however, rays are allowed to cross and the associated Eulerian functions are multi-valued. As a consequence, merging of two curves at the same level will never happen, they can instead intersect by simple superimposition. Self-intersection may also happen and is a more serious problem.

This research has been the source of many contacts and collaborations between geophysicists and applied mathematicians. We have tried to understand ideas and compare methods. In particular the "level set" philosophy of the applied mathematicians turned out to be radically opposed to decades of RT practice in geophysics. I must confess that in the early 1990's, I naively believed we would produce a general Eulerian GO solver and I clearly underestimated the difficulties. Even though viscosity solvers (i.e. first arrival Eulerian H-J solvers) are suitable and actually used in several context in the oil industry (see [46] for instance) no significant application of multi-valued (or multi-phase) Eulerian solvers has yet emerged in geophysics as there are yet no operant Eulerian algorithms able to solve truly complex problems more efficiently than RT even in two dimensions.

Eulerian GO remains nonetheless a fascinating research challenge with a potentially larger field of application than geophysics alone (see [14] [15] [45] for a plasma application for instance). This paper is more an introduction to the topic (as I see it) than a real review of the field. Still, it gives a flavor of the different approaches (that I am aware of) undertaken in the last ten years. Of course it does not pretend to be extensive and complete (I apologize for any omission). It must be understood that it is a personal interpretation of these methods and cannot be substituted for the original technical content of the reviewed articles. It is therefore potentially subject to inaccurate or incomplete descriptions. I also have seized this opportunity to sketch minor unpublished works when they fit.

The paper is organized in three parts. The first three sections introduce the mathematical models that are usually used in this literature. We stick to the 2-D case where one dimension

can be interpreted as a propagating direction and assimilated to time. It simplifies the presentation and still exhibits the complexity that makes Eulerian GO a difficult problem. Then we quickly review the numerics behind RT and some of its more sophisticated version and give basic information on viscosity single-valued solutions and their computations (two sections). The final four sections present the different categories of Eulerian GO numerical methods.

1   Mathematical Models

1.1   The Hamiltonian system and Calculus of Variation

The classical 2-D two-point ray tracing problem consists in finding all (say C^2) curves

$$
\begin{aligned}
[0,t] &\rightarrow \mathbb{R}^2 \\
s &\mapsto y(s)
\end{aligned}
$$

between two prescribed end-points $y(0) = y_0$ and $y(t) = y_t$ that minimize (possibly locally) the "action"

$$
\int_0^t \frac{1}{c(y(s))} \|\dot{y}(s)\| ds \tag{1}
$$

where $\dot{(.)} = \frac{d(.)}{ds}$. The integral is the physical length weighted by the inverse of a strictly positive smooth speed function c, hence a time for the signal to travel, the "travel-time", between end-points. The optimal curves, called rays, are constrained at both end and satisfy a set of ordinary differential equation given by the classical Euler-Lagrange equations of the calculus of variation [84] [42].

In a typical geophysical application, travel-times have to be calculated for many "source-receiver" pairs of point. As the actual computation of two point rays is difficult because of the end-point constraints, a different problem is generally considered : the final $y(t) = y_t$ constraint is relaxed but the curves are allowed to depend on a parameter that can either represent their initial direction (or angle) in the case of an isotropic source point or simply the initial position $y(0) = y_0$, where y_0 spans a given source sub-manifold. We may explicitly write the dependence $y(s, y_0)$ in the sequel. We concentrate on the second case. The action can be made slightly more general by the addition of a given initial travel-time function ϕ^0

$$
\int_0^t \frac{1}{c(y(s, y_0))} \|\dot{y}(s, y_0)\| ds + \phi^0(y_0),
$$

and we now also minimize with respect to the initial position of the curve. Then the optimal curves satisfy a classical initial value problem with initial conditions depending on y_0 and ϕ^0. Note that we can interpret every individual ray as a two point ray by fixing a posteriori the end-points. The idea is therefore to propagate, or "shoot", a large number of rays from

the source region in order to cover as well as possible the receiver region. Standard ODE solvers can be used to do so (see section 2).

We will use a further simplification throughout this paper and refer to it as the *paraxial* model. It consists in a dimensional reduction of the problem when the physical situation is such that rays propagate along a privileged axis usually denoted z (for depth) in geophysics. More precisely we assume that no ray can turn back in the z direction. Then, z can be used to parameterize the curves instead of s. As a consequence, we can work with 1-D curves :

$$
\begin{aligned}
[0, z_f] &\rightarrow \mathbb{R} \\
z &\mapsto y(z)
\end{aligned}
$$

representing the horizontal position of the ray at depth z and z_f is a given final depth. The action now writes

$$
\int_0^{z_f} \frac{1}{c(y(z, y_0))} \sqrt{1 + \dot{y}(z, y_0)^2} \, dz + \phi^0(y_0)
$$

where $\dot{(.)} = \frac{d(.)}{dz}$. In this configuration $y_0 \in \mathbb{R}$ spans the surface $z = 0$. The rays are the y solutions of the 1-D Hamiltonian system (throughout the paper the z and s notations are equivalent)

$$
\begin{cases}
\dot{y}(s, y_0) = H_p(s, y(s, y_0), p(s, y_0)), \ y(0, y_0) = y_0, \\
\dot{p}(s, y_0) = -H_y(s, y(s, y_0), p(s, y_0)), \ p(0, y_0) = \phi^0_{y_0}(y_0),
\end{cases}
\tag{2}
$$

where the Hamiltonian function H is given by

$$
H(s, y, p) = -\sqrt{\frac{1}{c^2(s, y)} - p^2},
\tag{3}
$$

c may depend on s as it is a physical dimension (z), H_y and H_p are the partial derivatives of H. The couples (y, p) are called bicharacteristics and live in phase-space, here simply $\mathbb{R}_s \times \mathbb{R}_y \times \mathbb{R}_p$. The travel-times are solutions of

$$
\dot{\varphi}(s, y_0) = p(s, y_0) \cdot H_p(s, y(s, y_0), p(s, y_0)) - H(s, y(s, y_0), p(s, y_0)),
$$

$$
\varphi(0, y_0) = \phi^0(y_0).
\tag{4}
$$

The travel-time, also called phase, $\varphi(s, y_0)$ is therefore transported by the corresponding ray $y(s, y_0)$. When rays are crossing, the travel-time is a a multi-valued function of the domain spanned by the rays.

1.2   High frequency wave equation approximation

The other classical derivation of GO is based on the WKB approximation of a linear wave equation. Let us consider for instance the Helmholtz equation

$$\Delta u(X) + \frac{\omega^2}{c^2(X)} u(X) = 0. \tag{5}$$

To be consistent with the previous section, let us take $X = (z, x)$ where x represents the horizontal axis $y(z)$ is living on. We now assume that equation (5) is set on the half-plane $\mathbb{R}_z^+ \times \mathbb{R}_x$ with a Dirichlet boundary condition

$$u(0, x) = a_0(x) e^{i\omega \phi^0(x)} \tag{6}$$

on $z = 0$ and ad-hoc radiation boundary conditions at infinity.

For high frequencies ω, the oscillatory behavior of the solution generally makes the direct numerical resolution of (5) too expensive even in two dimensions. Fortunately, when the scale of the variations of $\frac{1}{c}$ are much smaller than the wavelength, it is relevant to use a WKB approximation of u [35] [30]. Let us recall briefly the principle of this approximation before discussing numerical methods in this framework. The solution of (5) is a priori replaced by the following asymptotic expansion

$$u = (a + \frac{a_1}{i\omega} + \frac{a_2}{(i\omega)^2} + \dots) e^{i\omega \phi} \tag{7}$$

called the WKB ansatz. After plugging this expansion in equation (5), we find at the leading significant orders ω^2 and ω the Eikonal equation for the phase ϕ

$$\|\nabla \phi\|^2 = \frac{1}{c^2} \tag{8}$$

(where $\nabla \phi = (\phi_z, \phi_x)$) and the transport equation for the amplitude a

$$2\nabla a \cdot \nabla \phi + a\Delta \phi = 0. \tag{9}$$

The structure of the ansatz $u \simeq a e^{i\omega \phi}$ automatically takes into account the oscillations. The approximation of the solution of (5) now relies on the resolutions of (8)-(9).

The classical method is Lagrangian and applies an "inverse level-set" strategy : one simply notices that the integral curves of $\nabla \phi$, again called rays and denoted $Y(s)$ (i.e. $\frac{dY}{ds} = \nabla \phi(Y(s))$ and s is a parameterization of the curve) are solutions of a simple system of ordinary differential equations (ODEs)

$$\frac{dY}{ds} = P(s), \quad \frac{dP}{ds} = \frac{1}{2} \nabla (\frac{1}{c^2}(Y(s)) \tag{10}$$

(set $P(s) = \nabla\phi(Y(s))$ and use (8)). The phase $\phi(X)$, can be computed as the integral of $\|P\|^2$ along a ray $Y(s)$, since

$$\frac{d}{ds}\phi(Y(s)) = \frac{dY}{ds}.\nabla\phi(Y(s)) = \|P(s)\|^2 \qquad (11)$$

Notice that (10-11) enters the Hamiltonian framework (2-4) in 2-D with the Hamiltonian function

$$H(Y, P) = \frac{1}{2}(\|P\|^2 - \frac{1}{c^2(Y)}). \qquad (12)$$

Using the paraxial simplification of section 1.1, we can re-parameterize Y as $Y(s) = (z, y(z))$ and then (10-11) can be reduced to (2-4). The initial conditions are recovered from the identification of (6) with the ansatz (7).

1.3 Amplitudes

The Lagrangian resolution of (9) is a bit more involved. We just summarize here the main ideas. A complete and compact presentation of this topic can be found in [12] where other models are proposed for the computation of the amplitude. It consists in writing equation (9) as a conservation law and integrate it over a "tube" of ray. A tube is a domain formed by the rays $y(s, y_0)$ issued from an initial ball $y_0 \in B(\bar{y}_0, \epsilon)$, $\bar{y}_0$ being the initial position of a central ray and also bounded in s (say $s \in]0, t[$). One can then let ϵ goes to 0 to establish the conservation equation (we use the paraxial model)

$$a^2(0, y(0, \bar{y}_0))|\frac{\partial y(0, \bar{y}_0)}{\partial y_0}|\frac{1}{c(0, y(0, \bar{y}_0))} = a^2(t, y(t, \bar{y}_0))|\frac{\partial y(t, \bar{y}_0)}{\partial y_0}|\frac{1}{c(t, y(s_1, \bar{y}_0))}. \qquad (13)$$

Thus, knowing the amplitude at $s = 0$ gives the amplitude along the ray at all later "times" $s = t$:

$$a^2(t, y(t, \bar{y}_0)) = a^2(0, y(0, \bar{y}_0))\frac{c(t, y(s_1, \bar{y}_0))}{c(0, y(0, \bar{y}_0))}|\frac{\partial y(0, \bar{y}_0)}{\partial y_0}| (|\frac{\partial y(t, \bar{y}_0)}{\partial y_0}|)^{-1} \qquad (14)$$

provided $|\frac{\partial y(t, \bar{y}_0)}{\partial y_0}|$ does not vanishes. This happens in particular at caustics which are the points on the rays where an infinitesimal tube of neighboring rays collapses. This is actually the mathematical definition of a caustic point : a ray $y(s, y_0)$ encounters such a point when the determinant of the Jacobian matrix of y with respect to y_0 (here simply a scalar) is 0. This quantity is called "geometric spreading" as it provides a local measure of the geometric convergence or divergence of the rays. At caustics points (14) predicts an infinite amplitude, an artifact of the high frequency approximation. This is what people generally imply when they say that GO fails at caustics.

1.4   Computing amplitudes and localizing caustics

Caustics being an important ingredient of multi-valuedness and therefore of our problem, it is important to understand how they can be evaluated. The computation of $\frac{\partial y(s,y_0)}{\partial y_0}$ is performed using a set of additional ODEs obtained via a linearization of the system (2) with respect to y_0 :

$$
\begin{cases}
\begin{pmatrix} \dfrac{\dot{\partial y}}{\partial y_0}(s,y_0) \\[4mm] \dfrac{\dot{\partial p}}{\partial y_0}(s,y_0) \end{pmatrix} = A(s, y(s,y_0), p(s,y_0)) \cdot \begin{pmatrix} \dfrac{\partial y}{\partial y_0}(s,y_0) \\[4mm] \dfrac{\partial p}{\partial y_0}(s,y_0) \end{pmatrix}, \\[10mm]
\begin{pmatrix} \dfrac{\partial y}{\partial y_0}(0,y_0) \\[4mm] \dfrac{\partial p}{\partial y_0}(0,y_0) \end{pmatrix} = \begin{pmatrix} Id_{d \times d} \\[4mm] \frac{\partial^2 \phi^0}{\partial {y_0}^2}(y_0) \end{pmatrix}
\end{cases}
\tag{15}
$$

where

$$
A(t,y,p) = \begin{pmatrix} H_{py}(s,y,p) & H_{pp}(s,y,p) \\[2mm] -H_{yy}(s,y,p) & -H_{yp}(s,y,p) \end{pmatrix}.
\tag{16}
$$

Finding a caustic point on a ray therefore consists in solving (2-15). When $|\frac{\partial y}{\partial y_0}|$ vanishes or more precisely changes its sign, the ray has passed a caustic point.

Let us point out (for further use) that, as solutions of (15) with non-zero initial conditions, $\frac{\partial y}{\partial y_0}(s,y_0)$ and $\frac{\partial p}{\partial y_0}(s,y_0)$ cannot vanish simultaneously. Indeed, they satisfy (15) with non zero initial conditions. One can equivalently notice that a tube of *bicharacteristics* (i.e. in phase-space) has constant section. This property is also a consequence of Liouville's theorem (see [5]).

1.5   Examples of Multi-Valuedness

We now give two explicit examples of multi-valuednes which will be used to illustrate the Eulerian GO solvers.

The first (trivial) case involves rays issued from different sources. This occurs for instance when the boundary condition (6) is the sum of two waves :

$$
u(0,x) = a_{0,1}(x)e^{i\omega\phi^{0,1}(x)} + a_{0,2}(x)e^{i\omega\phi^{0,2}(x)}.
\tag{17}
$$

Let $c \equiv 2$ and $\phi^{0,1}(x) = x$, $\phi^{0,2}(x) = -x$ two independent initial phase functions for system (2-4). The analytical solutions are simple and consist in rays of slope 1 for the first function and slope -1 for the second (figure 1). Geometrical spreading is constant in both cases and
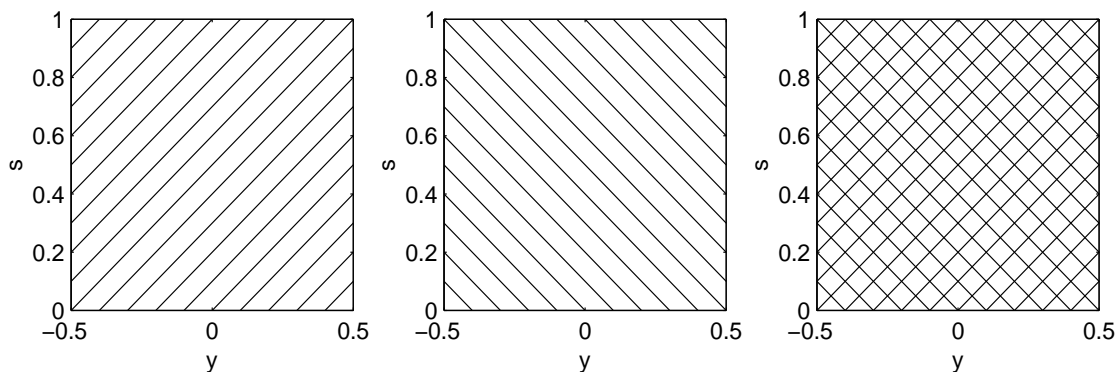
Figure 1: Left: Rays from the first source (shot from $s = 0$). Center : Rays from the second source. Right: superposition. Note this also represents fronts (normal to rays in this case).

so are the amplitudes. The level curves of travel-time are called the fronts and here are straight lines orthogonal to the rays. The linearity of the Hemlhotz equation ensures the GO solution to be the sum of these two contributions. The rays cross but it is a simple superimposition (figure 1). There is absolutely no interference between the two single valued GO solutions and they can indeed be simulated either with rays but also by solving (8) twice, once for each source.

More problematic is the case of a caustic formed either by focusing initial conditions or variations of the speed c that bends the rays. It is of course impossible to know a priori *when* and *where* a caustic will appear but differential geometry tells you *how*. It also provides information on the possible structures of multi-valued solutions (see [7] [6] [33] [49]).

In this theory, the set of bicharacteristics strips $\Lambda = \{(s, y(s, y_0), p(s, y_0)); (s, y_0) \in \mathbb{R}_s^+ \times \mathbb{R}_y\}$ is considered as a (Lagrangian) sub-manifold of co-dimension 1 of phase-space $\mathbb{R}_s \times \mathbb{R}_y \times \mathbb{R}_p$. Next we need to introduce the canonical projection from phase-space to configuration space :

$$\Pi \; : \; \mathbb{R}_s^+ \times \mathbb{R}_y \times \mathbb{R}_p \; \longrightarrow \mathbb{R}_s^+ \times \mathbb{R}_y$$

$$(s, y, p) \; \longrightarrow (s, y).$$

In our first example Λ is actually the union of two disjoint sub-manifolds $\Lambda = \Lambda_1 \cup \Lambda_2$ associated with each source that simply superimpose when projected in s, y space. The associated phase function (travel-time) is automatically bi-valued.

In the caustic case, Λ folds on itself in the p dimension direction. The Lagrangian solution $\Pi(\Lambda)$ is multi-valued and the projection become singular on the fold. The projection of the
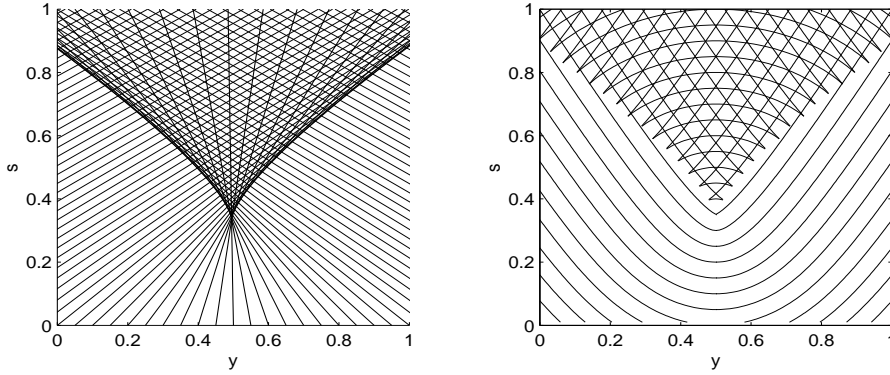
Figure 2: Left: Rays shot from $s = 0$. Right: Level curves of φ, the values of φ increase in the s direction.

fold is the caustic. Quite remarkably, differential geometry provide a generic classification of the different stable ways Λ can locally fold (stable means here that the structure described below of Λ cannot change under small perturbation in phase-space). More precisely, up to an unknown change of variable in phase-space which preserves the volume element $dy \wedge dp$, a local analytical description of Λ near multi-valued solution is given. In our 2-D case there are two possibilities where (s, p) are used to parameterize Λ : the Fold, $y = 3p^2$ and the Cusp, $y = 4p^3 + 2sp$ (which corresponds to the junction of two Folds). A similar but larger classification exists for higher dimensions.

A cusped caustic may be obtained using :

$$c \equiv 1, \ \phi^0(y^0) = \int_0^{y^0} \frac{p^0(x)}{\sqrt{1 + p^0(x)^2}} dx, \ \text{with } p^0(x) = \frac{-3(x - 0.5)}{\sqrt{1 + 3(x - 0.5)^2}}, \qquad (18)$$

Figure 2 shows the corresponding rays, solutions of (2), shot from $s = 0$ upwards. The cusped caustic can easily be distinguished as the curve which separates the multi-valued zone (where points are reached by three rays) and the single-valued zone (only one ray). In this case it is possible to solve analytically system (2) and represent the level curves of the Lagrangian phase for a continuum of rays. It is done on figure 2. The value of the phase increases from bottom to top. The level curves of the phase fold on themselves inside the caustic where the solution is multi-valued.

1.6   Lagrangian to Eulerian

It is also possible to recover the Eikonal equation (8) from system (2-4) using a Lagrangian to Eulerian transformation (basically the "level-set"method) :

As we proceed along the ray and as long as the "no caustic" property $\frac{\partial y}{\partial y_0}(s, y_0) \neq 0$ is satisfied, we can apply the local inversion theorem to the mapping $y_0 \to y(s, y_0)$. This implicitly means following a "level-set strategy" is legitimate : the Eulerian variable $\phi(s, x)$ evaluated at the Lagrangian coordinates specified by the rays matches the Lagrangian phase :

$$\phi(s, y(s, y_0)) = \varphi(s, y_0) \tag{19}$$

It is well defined in the domain spanned by the rays $y(s, y_0)$ as long as there are no caustics.

A classical result of the calculus of variation [42] [84] then states that :

$$\phi_x(s, y(s, y_0)) = p(s, y_0). \tag{20}$$

Note that the initial conditions in (2) satisfy (20). It is then straightforward to derive the Hamilton-Jacobi equation, first in Lagrangian coordinates and then back to Eulerian coordinates :

$$\begin{cases} \phi_s(s, x) + H(s, x, \phi_x(s, x)) = 0, \ for \ (s, x) \in \ \mathbb{R}_s^+ \times \mathbb{R}_y^d \\ \phi(0, y_0) = \phi^0(y_0), \ for \ y_0 \in \mathbb{R}_y^d. \end{cases} \tag{21}$$

Away from caustics, ϕ defined by (19) is called a classical solution of (21). We recall that we are working here under the paraxial model and that the rays propagate in a privileged s (or z) direction. As a consequence the phase can only increase in this same direction and ϕ_s is positive. We can therefore extract a square root in (8) to recover (21) with $H = -\sqrt{\frac{1}{c^2(s, y)} - p^2}$.

1.7 A paraxial limiter

A clever modification [71] [46] of H deserves to be mentioned. It leads to a systematic use of the paraxial model even when there exists rays that potentially turn backwards. We recall that $\nabla \phi = (\psi_s, \psi_x)$ gives the direction of the ray. If this direction makes an angle θ with the s axis, θ must satisfy (according to (8)) the relation

$$\psi_s(s, x) = \frac{\cos \theta}{c(s, x)}.$$

Then the assumption

$$\psi_s(s, x) \geq \frac{\cos \theta_{max}}{c(s, x)} > 0 \tag{22}$$

guarantees that the rays cannot deviate more than an angle θ_{max} from the s axis and therefore cannot turn back. Hence the idea to modify the Hamiltonian function to a finite aperture Hamiltonian :

$$H^\theta(s, x, p) = -\sqrt{\max(\frac{1}{c(s, x)^2} - p^2, (\frac{1}{c(s, x)} \cos \theta_{max})^2)}. \tag{23}$$

This Hamiltonian cuts off parts of the solution associated with rays that make an angle higher than θ_{max} with the privileged s-axis direction. It replaces them by a plane wave propagating in the θ_{max} direction. It therefore prevents numerical problems, should $\frac{1}{c(t,x)}^2 - p^2$ become negative thus indicating a turning ray.

1.8 (s,p) Maslov projection

Let us come back to the Fold. Multi-Valuedness is a consequence of the projection Π of the Lagrangian submanifold described by $y = 3p^2$ on the (s,y) space (section 1.5) : each point y is associated with two p-branches : $p = \pm\sqrt{(\frac{y}{3})}$. It is important to notice, as Maslov did ([28] or [39] for a review), that a single-valued projection is still possible but onto (s,p) space. Actually we know more : $\frac{\partial y}{\partial y_0}(s,y_0)$ and $\frac{\partial p}{\partial y_0}(s,y_0)$ cannot vanish simultaneously. Therefore it is *always* possible to find a projection space (here (s,p)) where the phase is single-valued. The Maslov Lagrangian treatment of the amplitudes at caustics is therefore based on the resolution of equation (9) in (s,p) space. Geometrical spreading (as used in formula (14)) is replaced by $|\frac{\partial p}{\partial y_0}(s,y_0)|$. Two equivalent corrected transport equations (for each p-branch) in (s,y) can also be derived [63] and a weighted combination of the solution of both projection $((s,y)$ and $(s,p))$ has been proposed to yield a uniform solution [59].

In such a configuration, it makes sense to choose as the Eulerian configuration space, the space spanned by $p(s,y_0)$ instead of $y(s,y_0)$. As long as the p trajectories do not cross, i.e. $\frac{\partial p}{\partial y_0}(s,y_0) \neq 0$, it is possible to invert $y_0 \rightarrow p(s,y_0)$ and switch to Eulerian variables denoted (s,q) (the q Eulerian variable corresponds to the p Lagrangian variable) As before, we need a variable to describe the phase : $\phi(s,q)$ but also one to keep track of the position y which we denote $X(s,q)$:

$$X(s,p(s,y_0)) = y(s,y_0).$$

$$\phi(s,p(s,y_0)) = \varphi(s,y_0).$$

(24)

Now, simply deriving the above formulae with respect to s and with the help of the Hamiltonian system (2), we can establish that X and ϕ satisfy in Eulerian coordinates (s,q) the equations :

$$\begin{cases} X_s(s,q) - H_y(s,X(s,q),q) \cdot X_q(s,p) = H_p(s,X(s,q),q), \\ \phi_s(s,q) - H_y(s,X(s,q),q) \cdot \phi_q(s,q) = q \cdot H_p(s,X(s,q),q) - H(s,X(s,q),q) \end{cases}$$

(25)

the initial conditions are deduced from (24).

1.9 The Kinetic model and the Wigner transform

It is also of course, always possible to perform the Lagrangian to Eulerian transformation in the full phase-space where there cannot be caustics. The Eulerian phase function $\phi(s,x,q)$

is always well defined by

$$\phi(s, y(s, y_0), p(s, y_0)) = \varphi(s, y_0) \tag{26}$$

and satisfies

$$\phi_s(s, x, q) + H_p(s, x, q) \cdot \phi_x(s, x, q) - H_y(s, x, q) \cdot \phi_q(s, x, q) = \\ q \cdot H_p(s, x, q) - H(s, x, q). \tag{27}$$

When working in higher dimensions (2 or 3), the q variable can advantageously be replaced by $\frac{\hat{q}}{c(s,x)}$ where $\hat{q}$ lives on the unit sphere [36] [37] [29]. We indeed know (see section 1.3) that the bicharacteristics (Y, P) and therefore the solution of (27) live on the hyper-plane $\|P\| = \frac{1}{c(s,Y)}$.

A kinetic approach to GO where rays can be considered as the trajectories of particles in phase-space yields a similar equation. Let us define the density function of a family $(y_i(s), p_i(s))_{i=1,\ldots,,N}$ of N such particles as

$$f(s, x, q) = \sum_{i=1}^{N} a_i \delta(x - y_i(s)) \delta(q - p_i(s)) \tag{28}$$

where δ is the Dirac mass and a_i can be interpreted as the "weight" of the particle and could depend on s in a more sophisticated model. The dynamics of the particles being governed by (2), $f(s, x, q)$ satisfies the following kinetic equation

$$f_s(s, x, q) + H_y(s, x, q) \cdot f_x(s, x, q) - H_p(s, x, q) \cdot f_q(s, x, q) = 0. \tag{29}$$

Note (29) can be derived from Helmholtz equation (5) using semi-classical limits [16] [25] (see also [43] in the bounded domain case). This theory, based on the Wigner transform is well known in the study of Schrödinger equations [61]. In the 2-D setting of section 1.3, the Wigner density $w_\omega(X, P)$ is the fourier transform of a delocalized quantity :

$$w_\omega(X, \Xi) = \mathcal{F}_{Z \to \Xi}(u(X + \frac{1}{2\omega}Z)\overline{u(X - \frac{1}{2\omega}Z)}) \tag{30}$$

Under the paraxial model simplification where (X, Ξ) is replaced by the reduced coordinates (s, x, ξ), the limit $w_\infty = \lim_{\omega \to +\infty} w_\omega$ can be shown to satisfy in a weak sense equation (29). The link between the weak limit of the Wigner measures and multi-valued GO is also studied in [64] [51] in which it is established (still in a weak sense and away from caustic points) that

$$(w_\infty(s, x, \xi) =) f(s, x, \xi) = \sum_{k=1}^{np} a_k(s)\delta(\xi - p_k(s)), \tag{31}$$

where np is the number of bicharacteristics $(y_k(s), p_k(s))$ such that $y_k(s) = x$. In this model $a_k(s) = a(y_k(s))^2$ is the square of the amplitude, solution of (9) and carried by the kth ray.

2 Lagrangian numerical methods

The numerical resolution of the system of ordinary differential equations (2-4) (generally coupled to (15)) is usually performed using standard Runge-Kutta solvers that are now commonplace in academic and commercial software packages (we will not describe this type of technique here). There also exist "simplectic" solvers that preserve (or try to preserve) the Liouville conservation property of each volume element $dy \wedge dp$ (See [47] for a review). The numerical difficulties are linked to the format either of the given speed function or of the output.

The speed is commonly given sampled on a grid. The solver then obviously needs an interpolation method as it does not necessarily evaluate the right-hand side of the system at grid points. The most common technique seems to be the use of splines. Notice that the "level-set"/Eulerian approach does not directly encounter this problem if grid discretization of the equation matches the sampling grid for the speed. The interpolation then occurs automatically at the level of the solution through the discretization of the equation. Of course, if the grid discretization of the equation does not match the sampling grid then interpolation is also needed.

At the other end of the numerical procedure, travel-times and other quantities such as geometrical spreading are generally required at a large number of receiver points that are not necessarily reached by the rays that have been shot whatever the number. Interpolation is then again needed. There are several approaches to the problem (see [24] for a short introduction).

The wavefront construction method [82] evolves in s a representation of $\{y(s, y_0)/y_0 \in D\}$ (D being an initial set of rays) using a finite number of rays $(y(s, y_{0,i}))_{i=1..nr}$ that retain their initial neighbor connectivities. It is then possible to compute a mesh surface of the wavefront and of the travel-time field above even if the solution is multi-valued (rays cross and the surface folds). Mesh cells can collapse or conversely become so large that inter-polating travel-times may be inaccurate. Several techniques have been proposed either to improve interpolation or to provide a criterion for the elimination and division of cells. I refer to [23] [66] [83] [58] [62] for more details about these Lagrangian practices.

Let us finally mention that the numerical resolution of large 3-D problems may be time consuming. As each ray can computed independently the parallelization of the computation of a large number of rays is also used.

3 Eulerian viscosity solvers

3.1 Viscosity solution

In the presence of a caustic there is still a notion of weak single-valued solution for equation (21) called "viscosity solution" [31] [9]. Viscosity solutions are worth considering because any stable numerical scheme converges to this class of solution [77] [32]. These schemes are generally called upwind because they discretize space derivatives on the opposite side to the direction of the rays (would rays be traced).

A link can be made between Lagrangian and Eulerian viscosity solution using the theory of optimal control [11]. The viscosity solution can be characterized as the value function of the following optimization problem

$$\phi(s,x) = \inf_{\substack{\{y_0 \in \mathbb{R}_y,\ y(.) \in W^{1,+\infty}(\mathbb{R});\\ y(0)=y_0,\ y(s)=x\}}} \int_0^s L(t,y(t),\dot{y}(t))dt + \phi^0(y_0), \tag{32}$$

where the minimization is performed with respect to the admissible curves $y(.)$ and their initial point y_0. The "Lagrangian" function $L(s,x,v) = \sup_{p \in \mathbb{R}_p}\{p \cdot v - H(s,x,p)\}$ is the Legendre transform of H with respect to p. One can formally check that the Euler-Lagrange equations of this problem correspond to the Hamiltonian system (2). It means that the rays are the critical curves of the optimization problem (32) and the viscosity solution the optimal value of the cost function.

When each point is only reached by one ray, we have a single-valued classical solution and the value function of problem (32) is exactly the integral of the phase ODE in (2).

If more than one ray reaches the time space point (s,x) and if we denote $(y_{0,k})_{k=1..n}$ the n initial points of these curves, then the viscosity solution ϕ selects minimum of the associated phases :

$$\phi(s,x) = \min_{k=1..n} \varphi(s,y_{0,k}). \tag{33}$$

If there is a zone where no ray penetrates, the viscosity solution implicitly generates "non-classical" rays to fill this empty zone. It means that the optimal curves will still satisfy the Hamiltonian system (2) but not necessarily the original initial conditions (see [13] for more on this phenomena). When the configuration space is bounded, the optimal curves may only satisfy the ray equations (2) piecewise (they can be reflected or diffracted) or they can creep along boundaries. These interesting situations are probably linked to diffraction phenomena and should hopefully be investigated elsewhere.

The viscosity solution corresponding to our two examples in section 1.5 are presented in figure 3 and 4. They can be obtained by applying the minimum phase principle (33). It is
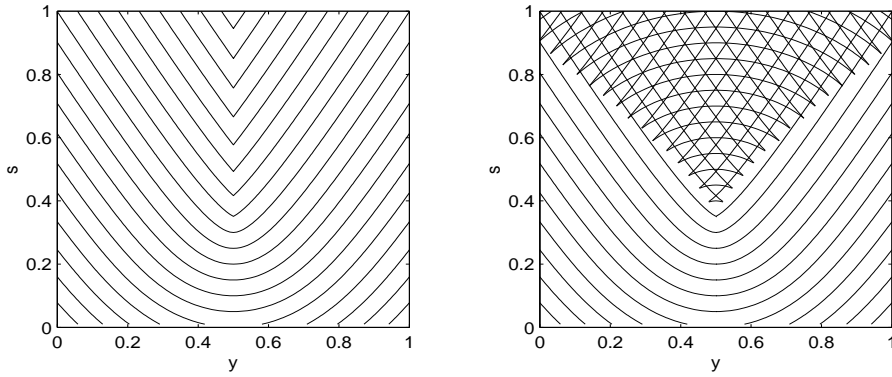
Figure 3: Left : Level curves of the viscosity solution ϕ with a kink on $y = 0.5$. Right : Level curves of the multi-valued solution φ.
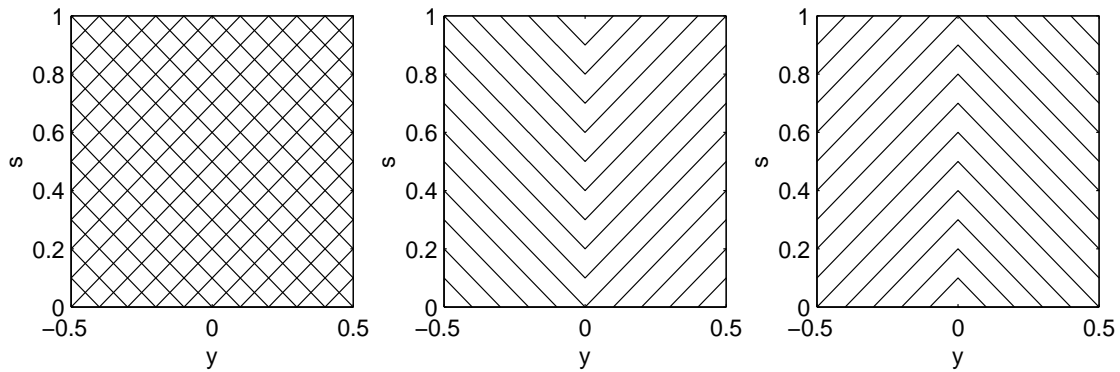

Figure 4: Left : Level curves of the multi-valued solution φ. Center : Viscosity solution level curves of the viscosity solution ϕ (first arrival) with a kink on $y = 0.5$. Right : Level curves of the remaining part of the multi-valued solution (second arrival).

easily interpreted because, when the speed c is constant, travel-time is proportional to the distance function. Both cases exhibit a vertical curve of singularities in the gradient of ϕ called a kink (or shock).

3.2   Upwind solvers

Convergence of numerical solvers towards the viscosity solution relies on theoretical properties (monotonicity, stability, etc..). The general proof of convergence for Hamilton-Jacobi equation is quite technical [77] [32] and I have not seen any simplification attempt in the case
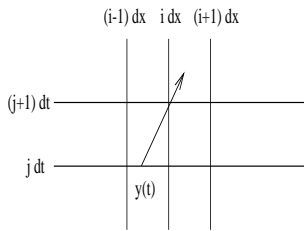
Figure 5: The ray reaching (s^{j+1}, x_i) $(dt = ds)$.

of the Eikonal equation (even for constant speed). I show here how the standard Godunov solver can be derived in a simple case. This derivation gives a good intuition of what upwind solvers amount to.

Let us take $H(s, x, p) = -\sqrt{1 - p^2}$ (i.e. does not depend on (s, x) and $c \equiv 1$). The discretization points in s are denoted $(s^j = j\,ds)_{j \in \mathbb{Z}^+}$ and $(x_i = i\,dx)_{i \in \mathbb{Z}}$ in x where ds and dx are fixed grid steps. The phase at grid points is $\psi_i^j = \psi(s^j, x_i)$. We focus on the behavior of the solution between s_j and s_{j+1} around point x_i. We further suppose that a continuous piecewise linear approximation of the phase is made (the viscosity solution can be shown to be $\mathcal{C}^0$) and denote $\psi_x^- = \frac{\psi_i^j - \psi_{i-1}^j}{dx}$ and $\psi_x^+ = \frac{\psi_{i+1}^j - \psi_i^j}{dx}$ the (constant) slopes of this approximation respectively on the left and the right of x_i, these are called the upwind derivatives. Remark that these quantities also give the slopes of rays $H_p(\psi_x^\pm) = \frac{\psi_x^\pm}{\sqrt{1 - (\psi_x^\pm)^2}}$ respectively on each side of x_i. We now consider a ray such that $y(s^{j+1}) = x_i$ and $y(s^j) < x_i$ (figure 5). We can exactly integrate (4) between on $]s^j, s^{j+1}[$ and find :

$$
\begin{aligned}
\psi(s^{j+1}, x_i) = \phi(s^{j+1}) \quad &= \phi(s^j) + \int_{s^j}^{s^{j+1}} p(s) H_p(s, y(s), p(s)) - H(p(s))\,ds \\
&= \psi(s^j, x_i) - (s^{j+1} - s^j) H(\psi_x^-)
\end{aligned}
\tag{34}
$$

which is a finite discretization of (21).

The problem now reduces to determining automatically the direction of the rays and deciding what should be done when rays converge (shocks or kinks) or diverge (rarefactions). Figure (5) shows the four possibilities to be considered : A. $H_p(\psi_x^-) \geq 0$, $H_p(\psi_x^+) \geq 0$. B. $H_p(\psi_x^-) \geq 0$, $H_p(\psi_x^+) < 0$. C. $H_p(\psi_x^-) < 0$, $H_p(\psi_x^+) \geq 0$. D. $H_p(\psi_x^-) < 0$, $H_p(\psi_x^+) < 0$. The front (level curve of phase $\psi = \psi_i^j$) is shown as a dashed line.

The sign of the upwind derivatives easily gives the direction of the ray and cases A and D are dealt with like in (34). Conversely we need an additional criterium to deal with situations B and D. Following the minimal phase property of the viscosity solution (33) we decide to select the minimal phase solution. It will be given by the ray with highest slope (in absolute value) for B (the side where the front, dashed line, is the closest to point s_{j+1}, x_i)). In case

C, there are no rays from (s_j, x_i) to (s_{j+1}, x_i) but using (32) and recalling that the phase is here the distance function, we postulate that the zone, uncovered by "classical" rays, is covered by a fan of "diffracted" or "virtual" rays from point (s_j, x_i). Minimum travel-time is then associated to the "virtual" ray with 0 slope (see also section 3.5 on this topic).

Using the monotonicity of H_p (H is strictly convex) the following formula automatically determines the correct upwind derivative in case A to D :

$$\psi_x^u = \text{modmax}(\max(\psi_x^-, 0), \min(\psi_x^+, 0)). \tag{35}$$

Here $modmax(a, b)$ return the highest module argument. The discretization of (21) then is

$$\psi(s^{j+1}, x_i) = \psi(s^j, x_i) - (s^{j+1} - s^j) H(\psi_x^u). \tag{36}$$

One can convince himself (by writing it down case by case) that (36) is actually a simplified version of the general Godunov solver for p convex Hamiltonians that reach minimum value at 0 [69] :

$$H^G(\psi_x^-, \psi_x^+) = ext_{\psi \in I(\psi_x^-, \psi_x^+)} H(t_j, x_i, \psi) \tag{37}$$

where $I(a, b) = [\min(a, b), \max(a, b)]$ and ext defined by

$$ext_{\psi \in I(a,b)} = \left\{ \begin{array}{l} \min_{a \leq \psi \leq b} \ if \ a \leq b \\ \max_{b \leq \psi \leq b} \ if \ a > b \end{array} \right.$$

There are of course many other possibilities for both s and x discretization of (21). For more details you can go to this (incomplete) list of references : [69] [55] [77] [57] [52] [20].

Let us also mention less classical works: an HJ solver on unstructured grid [1] [2] [3], a specific grid refinement procedure [71] and an attempt at exploiting the linearity of Hamilton-Jacobi equations in the $(\mathbb{R} \cup +\infty, Max, +)$ algebra [40]. The derivation of a Godunov solver for the Eikonal equation in an anisotropic medium is given in [72].

3.3   CFL condition

The derivation also clearly shows why a CFL condition is needed and how it should be determined. To be valid, our reasoning requires that the "light cone" formed by rays reaching (s^{j+1}, x_i) and retro-propagated at "time" $s = s^j$ has support *inside* $[x_{i_1}, x_{i+1}]$. Assuming constant grid steps ds and dx, a global sufficient CFL condition is

$$dt < \max_p H_p(p) dt. \tag{38}$$

Notice that, if using the finite aperture Hamiltonian (23), (38) simplifies to

$$dt < \frac{dx}{\tan(\theta_{max})}.$$

3.4   More upwinding - 2-D stationary equation

The paraxial model (section 1.1) turns a 2-D problem into a 1-D evolution problem with Cauchy data : a space dimension is transformed into a "time" dimension. This simplification is however not always possible, especially for applications (such as in [73] [3] [48] ...) which rely on the "stationary" 2-D Eikonal equation (8) in a bounded domain with Dirichlet or Neumann boundary condition. The first possibility for solving this equation consists in looking for the stationary state of an evolution equation on a 2-D + time extended domain. The numerical solvers are then similar to those described in section 3.2. The second option is to derive a discrete stationary Hamilton-Jacobi equation by means of "local" upwinding. The discrete equation can be solved by several iterative methods [70] [73] and has been the base for the development of the "fast-marching" method [75] [76]. In this last method, one notices that it is not necessary to update the grid values at all iterations. More precisely, it is only necessary to sweep the domain following the rays. Several techniques designed to propagate (like a wavefront) a confidence band where points may need updating have been proposed ([75] [53]) thus reducing the computational cost of the method. I would like here to make two remarks : first the paraxial model relies on the same philosophy except that one knows a priori the direction this band should be propagated in. The "band" then reduces to its most simple form : a grid line. The second remark is that "fast-marching" in some sense is a Lagrangian sweep of the Eulerian grid while, in general, the equation derives from a "level-set" approach which precisely moves from a Lagrangian to a Eulerian description.

Even though the discrete 2-D model has been extensively used (in particular through "fast-marching" applications), nowhere have I seen its fully detailed derivation. I therefore give here, for the sake of completeness, a complement to [73]. It again illustrates, along the way, the "upwinding" philosophy.

The derivation of the discrete equation is based on the remark that the viscosity solution ψ of (8) satisfies the "optimal control" formulation:

$$\sup_{\|q\| \leq 1} \{\nabla\psi(x,y).q - \frac{1}{c(x,y)}\} = 0. \tag{39}$$

We use Cartesian coordinates (x,y) and skip all details about domain and boundary conditions. A regular grid discretization is introduced and $(x_i, y_j) = (i\,dx, j\,dy)$ denote the grid points, ψ_{ij} is the discrete approximation of ψ at (x_i, y_j).

A first order finite difference approximation is made in (39) and the equation is written at $x = (x_i, y_j)$.

$$\sup_{\|Q\| \leq 1} \{\frac{\psi((x_i, y_j) - dt\,Q) - \psi_{ij}}{-dt} - \frac{1}{c(x_i, y_j)}\} = 0 \tag{40}$$

dt is chosen such that $(x,y) - dt\,q \in](i-1)\,dx, (i+1)\,dx[\times](j-1)\,dy, (j+1)dy[$. Let us restrict ourselves to the first quadrant $]i\,dx, (i+1)\,dx[\times]j\,dy, (j+1)dy[$ on which we

approximate ψ using a "convex linear" combination of the value at grid points :

$$\psi((x,y) - dt\, q) = \alpha\, \psi_{ij} + \beta\, \psi_{i+1j} + \gamma\, \psi_{ij+1}$$

where α, β and γ are such that

$$\begin{cases} (x,y) - dt\, q = \alpha\,(x_i, y_j) + \beta\,(x_{i+1}, y_j) + \gamma\,(x_{i+1}, y_{j+1})) \\ \alpha + \beta + \gamma = 1. \end{cases}$$

The optimization problem (40) now depends on (α, β, γ). It can be worked out for the four quadrants and taking $dt = \frac{dx\, dy}{\sqrt{dx^2 + dy^2}}$ simplifies into the discrete Hamiltonian :

$$g_{ij}(D_x^- \psi_{ij}, D_x^+ \psi_{ij}, D_y^- \psi_{ij}, D_y^+ \psi_{ij}) = 0,\ \forall (i,j) \tag{41}$$

where

$$g_{ij}(a,b,c,d) = \sqrt{\max(a^+, b^-)^2 + \max(c^+, d^-)^2} - \frac{1}{c(x_i, y_j)},$$

$a^+ = \max(0, a)$, $b^- = \max(0, -b)$ and $D_x^- \psi_{ij} = \frac{\psi_{ij} - \psi_{i-1j}}{dx}$, $D_x^+ \psi_{ij} = \frac{\psi_{i+1j} - \psi_{ij}}{dx}$, $D_y^- \psi_{ij} = \frac{\psi_{ij} - \psi_{ij-1}}{dy}$, $D_y^+ \psi_{ij} = \frac{\psi_{ij+1} - \psi_{ij}}{dy}$.

The convergence of the discrete solution toward the continuous viscosity solution as the mesh size goes to zero is proved in [73]. Several iterative methods can be used to compute the discrete solution (ψ_{ij}), one popular choice being a relaxation method complemented by the "fast marching" strategy.

3.5   Source point simulation

The problem here is to simulate point source initialization (rays flowing in different directions from a single point) under the paraxial model where the natural Cauchy data initialization at $z = 0$ corresponds to one ray per point. When the source point (rays flowing isotropically in all directions) is located in a zone of constant speed C the analytical solution is known and we can set the initial condition away from the source point to avoid this problem.

This is however not always the case and I would like to explain here a practical application of the "rarefaction effect" observed in case C, figure 6. The phase $\psi(s^j, .)$ has a discontinuous gradient at $x = x_i$ that produces diverging rays on each side. As already noticed, there is a center zone which is not covered by the "classical" rays. The Lagrangian solution cannot take into account the singularity of the phase at $x = x_i$.

We therefore turn to the definition (32) of viscosity solutions to understand what the solution is. A simple way to force all paths to emanate from a given "source" point x_i is to use the initial phase function ϕ^0 to penalize all other points. For instance $\phi^0(x) = +\infty$, $\forall x \neq x_i$
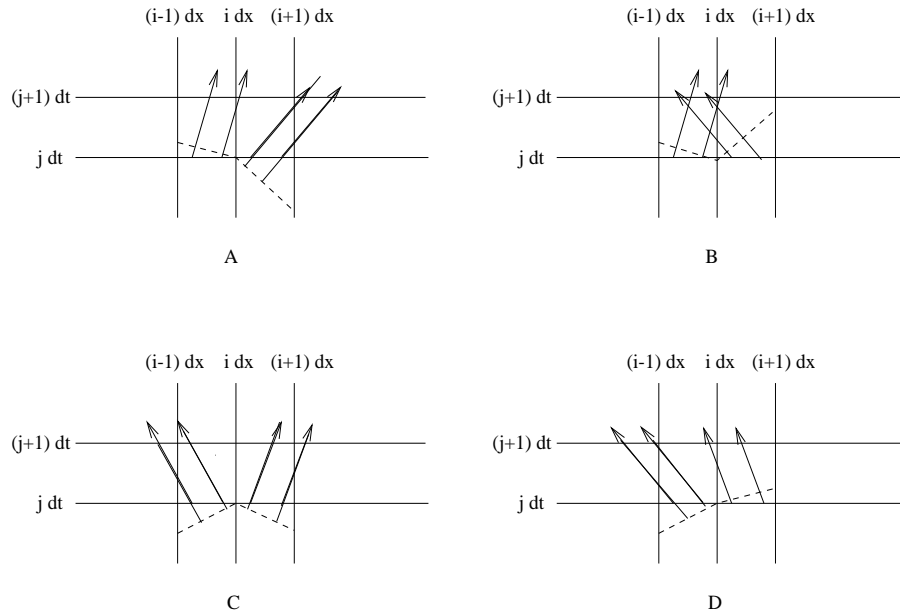
Figure 6: The four Riemann problem cases $(dt = ds)$.

and $\phi^0(x_i) = 0$ precisely achieves this goal. This last choice cannot be used in practice. A numerically safe way to approximate it is $\phi^0(x) = \alpha|x - x_i|$ where α is taken as big as possible. This precisely correspond to "rarefaction" case C discussed in section 3.2 where the slope of the rays is $\pm\alpha$. Because the gradient $\nabla\psi = (\psi_z, \psi_x)$ satisfies the Eikonal equation (8) α cannot exceed $\frac{1}{c}$ the inverse of the speed. From a numerical point of view, the CFL condition is even more stringent :

$$\frac{dt}{dx} < \frac{|\psi_z|}{|\psi_x|} = \frac{\sqrt{\frac{1}{c^2} - \alpha^2}}{\alpha}.$$

The initial phase $\phi^0(x) = \alpha|x - x_i|$ mimics a point source Lagrangian initialization by producing a fan of "ray" paths from x_i that fill the fan left empty by the classical diverging rays. The introduction of a singularity in the initial phase function therefore generates a point source initialization that would otherwise not be possible using the paraxial model.

A set of diverging rays, though not from a single point, can be initialized using $\phi^0(x) = \alpha|x - x_i|^2$. We can also introduce an ϵ parameter dependent smoothing of the singularity of $|x - x_i|$, the singular function being the 0 limit . The conjecture of the convergence as $\epsilon \to 0$ of the solution towards some diffractive wave phenomena is, it seems to me, an interesting one.

4   Eulerian multi-phase solvers - splitting methods

As explained in section 3.1, the computable viscosity solution is single-valued. The first obvious technique to compute a multi-valued GO solution by Eulerian means is to find a computable way to split this multi-valued solution into as many single-valued solutions as necessary. This turns out to be non trivial , essentially for geometrical reasons, and apparently cannot be done automatically without a priori knowledge of the structure of the multi-valued solution.

4.1   Caustic splitting of the multi-valued solution

We here assume that we are dealing with a cusped caustic. The multi-valued solution can be split into three single-valued branches delimitated by the caustic curve which corresponds to the projections onto (s, y) space.

In figure 7, we represent the three families of rays or portions of rays which are associated with each branch and in figure 8 the corresponding level curves of the phase. The left and right branches $(-Cl$ and $-Cr)$ are associated with the rays before they reach the caustic, the last branch $(+C)$ is given by the portions of rays once they have passed the caustic. A comparison with figure 3 shows that the viscosity solution is composed of the left branch $-Cl$ for $y \leq 0.5$ and the right branch $-Cr$ for $y \leq 0.5$ (they match on the kink $y = 0.5$). The viscosity solution therefore never "reaches" the caustic. By this we mean that the portions of rays implicitly associated with the viscosity solution do not reach the caustic (the notable exception is the singular tip of the caustic also called the cusp). Superimposing the three plots in each figure gives back respectively the complete family of rays and the multi-valued phase (figure 2).

Each branch separately can be shown to satisfy an optimal characterization like (32) and is interpreted as the viscosity solution of the Hamilton-Jacobi equation set in the domain corresponding to the actual support of the branch [11]. More precisely, if we denote ψ^{-Cl}, ψ^{-Cr} and ψ^{+C} the three branches of the phase, they individually satisfy equation (21) on their respective domain (represented on figure 8) bounded by the caustic. The initial conditions for the $-C$ branches are given by ϕ^0 and "out-going" or homogeneous Neumann boundary conditions can be used along the caustic. The $+C$ branch, which forms the remaining part of the multi-valued solution once the rays have passed the caustic, uses Dirichlet boundary conditions $\phi^{+C} = \phi^{-Cl}$ on the right part of the caustic and $\phi^{+C} = \phi^{-Cr}$ on the left part.

4.2   Caustic localization

There have been several attempts to implement the branch splitting algorithm of section 4.1. The main difficulty is the localization of the caustic boundary, in our case a free boundary as it depends on the solution itself. In the original paper [11], I used an Eulerian version of the
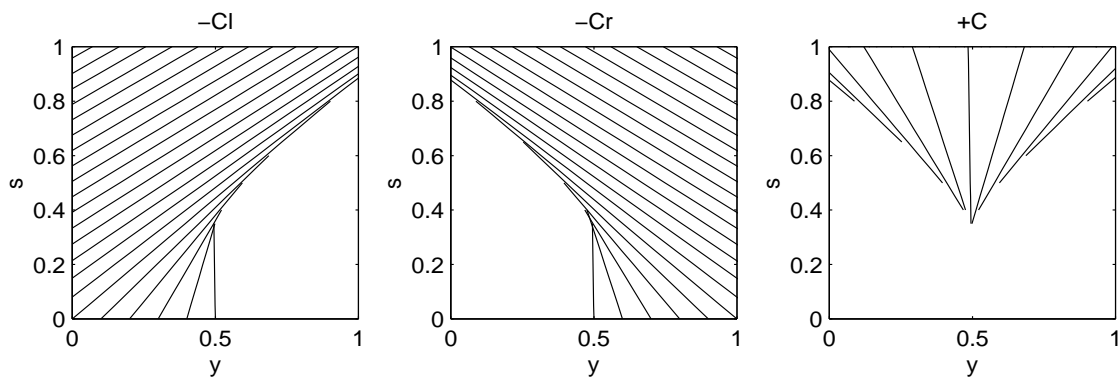
Figure 7: From left to right : the families of ray associated with the three different branches of the Lagrangian solution. The caustic is used to split the rays. In particular the branch $+C$ is made of the remaining parts of the rays of the branches $-C$s stopped at the caustic
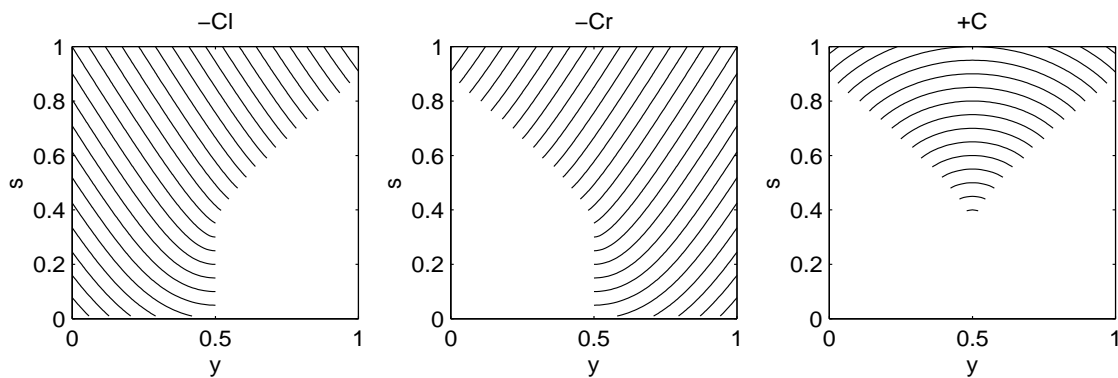

Figure 8: From left to right : The corresponding level curves of the phase. The values of the branches $-C$s and $+C$ match on their respective part of the caustic.

system of equation (15) coupled to the Eikonal equation (21) in order to detect the caustic boundary. This gave a set of Eulerian transport equations coupled to (21) for a variable $\beta(s, x)$ defined as

$$\beta(s, y(s, y_0)) = det(\frac{\partial y}{\partial y_0}(s, y_0)).$$

The method then consists of monitoring the position of the caustic by testing for 0 values of β. In practice there is no such thing as an exact 0 numerical value, hence the need to introduce a small tolerance parameter to localize the caustic. This causes inaccuracy as well as the necessary interpolation of the caustic curve on a grid.

This problem was solved in the case of a Fold caustic [14] (two branches) through the derivation of a specific equation for the caustic curve. Let $x_c(s)$ be the parameterization of the caustic. It satisfies the ordinary differential equation

$$\dot{x}_c(s) = H_p(z, x_c(s), p_c(s)) \tag{42}$$

where, at the continuous level, $p_c(s) = \phi_x^{-C}(s, x_c(s)) = \phi_x^{+C}(s, x_c(s)$ is the identical one-sided derivative of the two branches $\pm C$ connected at the caustic. It constitutes, coupled with the two $\pm C$ Eikonal equations, a closed Eulerian system for the GO Fold solution. At the numerical level things are not so straightforward. The phase will typically behave as $\pm\sqrt{x_c - x}$ near the caustic (we assume that the branches lie on the left of the caustic). It is therefore not possible to approximate p_c by simple upwind finite differences on one or the other branch. We nevertheless obtained a first order numerical closure in the form $p_c(s) \simeq 0.5 * (\phi_x^{-C}(s, x_c(s) - dx) + \phi_x^{+C}(s, x_c(s) - dx))$ (dx is a grid step) where now $\phi_x^{\pm C}$ can be safely approximated using finite differences. This numerical study is complemented by a moving grid strategy to adjust the domain to the caustic curve. The initial conditions for the $+C$ branch and the caustic are not necessarily given by the physics of the problem. We therefore designed an automatic initialization procedure for the system which does not interfere with the sought for solution. This Eulerian GO method has been used to compute High Frequency solutions of the Helmholtz equation in a plasma physics context [15].

Let us also mention a "time asymptotic method" [13] based on a local change of variable in "time" $\tilde{s}(s, x)$ that maps the caustic at $\tilde{s} = +\infty$. The Eulerian problem is then set on an unbounded domain and the solution is asymptotically stationary. This method has also been combined with the Fold equation method above [14] to derive an Eulerian method in the cusped caustic case (three branches) [10].

4.3   Shock-splitting

The hyperbolic conservation law community has a long experience of shock capturing. That is, finding precisely where the viscosity solution is discontinuous without tracing the characteristics. In the case of Hamilton Jacobi equations shocks are called kinks and are the locus

of discontinuous gradients. The viscosity solution remains continuous.

In [36], a method based on kinks detection is proposed. It relies on the idea that kinks are curves (in 2-D) where rays, that would otherwise cross, are terminated. The method can simply be illustrated on the superimposition case (figures 1 4) of section 1.5. The first step of the method consist in the computation of the viscosity solution (center plot of figure 1). It is then possible to detect numerically the kink, denoted K, (here the straight line $x = 0.5$) and store the trace of the (continuous) viscosity solution ψ_{visc} on K. It is then used as a Dirichlet boundary condition $\psi = \psi_{visc}$ on K for a new 2-D stationary Eikonal equation (8). We can assume here that we in fact have two problems on each half plane bounded by the kink with the same boundary condition. This new solution will be the second arrival depicted on the right plot of figure 4. It is important to realize that the phase data ψ on the kink curve K determines its tangential derivative and therefore also $\nabla \psi$ as the Eikonal equation (8) must be satisfied up to the boundary. Recalling that $\nabla \psi$ gives the ray direction, this second Eikonal resolution indeed continues the rays that have been shut off by the viscosity solution. No other initial or boundary conditions will interfere and give rise to multi-valuedness.

The limitation of this approach is clear when considering our second example of multi-valuedness. If we consider the viscosity solution associated with a cusped caustic, we observe as in the previous case a kink at $x = 0.5$. The rays flowing out of the kink to form the second part of the solution actually "fold" and live in a domain bounded on one side by the caustic. The solution is again multi-valued (two branches) and a new kink develops. The second step of the procedure as proposed in [36] will not see the caustic curve. The viscosity solution necessarily "fills" the zone behind the fold caustic, a similar phenomena to the source point procedure described in section 3.4. In this zone one observes the formation of artificial wavefronts which may interfere with the real solution and generate a new kink.

4.4   Segment projection

The segment projection method [37] originally developed for fluid mechanics application also is a caustic splitting approach. It uses two complementary representations of the GO solution that provides an overlapping mechanism over the caustics . The first representation decomposes the GO solution into single-valued branches, separated by caustics in the (s, y) space, called X-segments and represented each by $X(s, q)$ solutions of (25). The GO solution can also be split in a single valued branches separated by caustics in the (s, p) space. These branches are called P-segments. A similar Eulerian variable $Q(s, x)$ is needed and defined by

$$Q(s, y(s, y_0)) = p(s, y_0) \tag{43}$$

for their representation. Each P-segment therefore satisfies the equation (derived from (43))

$$Q_s(s, x) + H_p(s, x, Q(s, x)) \cdot Q_x(s, x) = -H_y(s, X(s, q), q). \tag{44}$$

The fundamental "Maslov" remark of section 1.8 now guarantees that a caustic cannot appear simultaneously in (s, y) and (s, p) space. As a corollary, we know therefore that the P-segments can be used to monitor the localization of the caustic boundaries and the apparition of new caustics in (s, y) space and symmetrically the X-segments are used in (s, p) space.

More practically, let us consider an (s, y) fold caustic curve located at $(s, x_c(s), p_c(s))$ in phase-space which "links" two X-segments on each side of $q = p_c(s)$. There cannot be an (s, p) caustic at $(s, x_c(s), p_c(s))$, we therefore know that a P-segment $Q(s, x)$ is well defined in a neighborhood of $(s, x_c(s))$. Actually we have $Q(s, x_c(s)) = p_c(s))$ and $x_s(s)$ is locally characterized by $Q_x(s, x_c(s)) = 0$. The P-segment can therefore be used to update the q position of the caustic defining the boundary for the associated X-segments. The same criterion can be used to detect the occurrence or disappearance of an (s, y) caustic thus leading to the splitting of an X-segment in two or the merging of two X-segments into one.

In the 1-D paraxial model, each P-segment is therefore associated at most with two X-segments and each X-segment with two P-segments as the same procedure is applied to (s, p) caustics. The main numerical issue is therefore to maintain a table of correspondence between segments. The method has been successfully applied to multi-valued GO solution consisting of several successive cusped caustics. Its main drawback is its computational cost, similar to RT.

5 Eulerian multi-phase solvers - a matching method

Slowness matching [78] can be thought of as a domain decomposition method. The domain is decomposed into non overlapping sub-domains and the different branches are sorted out by checking "matching" conditions at the interface between Eulerian single valued solutions of (21) on each sub-domain. We describe below the matching condition and how these Eulerian solutions are generated. The method is designed to solve in an Eulerian fashion the problem of finding all travel-times of rays between a source point and a sets of "receivers". Notice that the problem is "time" reversible as travel-time does not depend on the direction of the ray.

We stick to the simplest configuration and describe the algorithm first in the continuous setting : The Eulerian GO problem is solved, under the paraxial model simplification, between $z = 0$ and $z = 1$ (rays are flowing in the privileged z direction). We further assume that rays may cross but only at depth lines $z = 0$ or $z = 1$ where the source and "receivers" are located (i.e. the receivers are at $z = 1$). We consider two sub-domains separated by the interface set at $z = z_i$, the $0 \leq z \leq z_i$ domain is referred to as the bottom sub-domain and the $z_i \leq z \leq 1$ as the top sub-domain. We denote ψ_{up} the solution of (21) in the bottom domain with initial condition $\phi^0(x) = \alpha|x - x_0|$ at $z = 0$ that simulates an isotropic point source at x_0 (see section 3.5 on Eulerian point source initial conditions). It is naturally associated with rays traveling upwards from $z = 0$ to $z = z_i$. Similarly $\psi_{dn}^{x_1}$ denotes the

solution of (21) in the top domain with the same initial condition, $\phi^0(x) = \alpha|x - x_1|$, but this time set at $z = 1$. It means that the z "time" evolution is run backward from $z = 1$ to $z = z_i$ for the top solutions and associated rays travel downwards. As rays are supposed not to cross inside the domain (they actually only cross at source points) a family of singled valued Eulerian solutions $(\psi_{dn}^{x_1})$ indexed by the source location x_i can be computed in the top domain.

The method then consists in finding for all (receivers) source points x_1 the slowness vectors that "match" at one or more points x_m on $z = z_i$:

$$\nabla \psi_{dn}^{x_1}(z_i, x_m) = -\nabla \psi_{up}(z_i, x_m). \tag{45}$$

We recall that $\frac{dY}{ds} = \nabla\phi(Y(s))$ (section 1.2) is the direction of the ray, also called slowness vector. Condition (45) is the indication that two portions of ray match in position and speed. It is the Eulerian indication that there is a ray traveling from $(0, x_s^{dn})$ to $(1, x_s^{up})$ through $(0.5, x_m)$ and the total travel-time is the sum of travel-times on each sub-domain $\psi_{dn}^{x_s^{dn}}(0.5, x_m) + \psi_{up}^{x_s^{up}}(0.5, x_m)$. There are as many rays as matching points x_m. Under the paraxial model $\nabla\psi = (\sqrt{\frac{1}{c^2} - \psi_x^2}, \psi_x)$ and the matching condition (45) simplifies to finding the roots x_m of equation

$$\partial_x \psi_{dn}^{x_1}(z_i, x_m) + \partial_x \psi_{up}(z_i, x_m) = 0. \tag{46}$$

After discretization, travel-times and finite difference approximations of derivatives are only known at grid points. The matching condition (46) can only be satisfied in some "discretized" sense through interpolation or other root finding method. A common choice is also to let x_1 vary over the discretization grid.

In order to obtain a more general method, it is possible to relax the single-valued condition in the upper domain. The algorithm is then applied recursively : we first set z_i such that the solution is single valued in the bottom domain $0 < z < z_i$. If ray crossings occur in the top domain, apply the algorithm to the top domain : the initial condition is set at $z = z_i$ with initial condition $\psi^{up}(z_i, .)$ and a new interface is determined such that the solution is single valued in the bottom domain. A recursive depth search is also necessary to build a tree of matches and compute all travel-times. The simplest decomposition is to consider successive horizontal strips made of one horizontal grid line as the bottom sub-domain.

This method may seem complicated and the cost of many Eulerian solutions and slowness matchings prohibitive. One must keep in mind however that it computes the travel-times between all two points rays between a source point and a family of "receivers". In this respect the computational costs worked out in [78] indicate that the method is competitive.

6 Eulerian phase-space solvers and capturing methods

As mentioned in section 1.9, it is also possible to write an Eulerian equation either for the phase $\phi(s, x, q)$ (27) or a "density" of particles $f(s, x, q)$ (29). In both cases the main variable is defined over an Eulerian representation of the full phase-space $\mathbb{R}_s \times \mathbb{R}_y \times \mathbb{R}_p$. We already discussed the advantage of this approach : there are no caustics and no multi-valuedness in this space (section 1.8). Even though the q variable can be changed for an angle (section 1.8) the drawback, using such equations, is the dimension and thus the cost of the problem. In this paper where we treat a 2-D GO problem under a paraxial dimensional reduction, phase space is three dimensional (3-D). The full 2-D stationary problem corresponds to a 4-D phase-space. A 3-D GO model will lead to 6-D phase-space (5-D if paraxial). The challenge therefore is to find ways to reduce the dimensionality of the problem.

6.1 Full phase-space solvers

In [29] the authors combine different techniques but the model basically remains (29). The problem is to track a 1-D curve representing the front in a 3-D phase-space. The curve is modeled as the intersection of two 2-D surfaces which are advanced using a fast level set method. Details including, in particular, the initialization (and re-initialization when necessary) of the intersecting surfaces and cost estimates are given in [29] as well as 2-D and elementary 3-D test cases.

The approach pursued in [41] starts from the stationary form of the Eulerian phase-space equation (27). The idea of propagating a front is temporarily dropped. An "escape" stationary equation is solved in which the Eulerian variable represents at each phase-space point the travel time to exit a bounded phase-space domain following the Hamiltonian dynamics (2). The corresponding Lagrangian problem would amount to shoot rays from all phase-space points in the domain (point sources everywhere). The result can therefore be used to evolve any initial condition that forms a curve in phase-space. The fast marching method is then adapted to solve this phase-space PDE.

6.2 Moment methods

It is common practice in kinetic theory to consider quantities, averaged in "speed" q, called moments : $m_k(s, x) = \int q^k f(s, x, q) dq$. When the p dependence of the Hamiltonian is in the form (see [27])

$$H(s, x, p) = \frac{1}{2}p^2 + V(s, x) \tag{47}$$

with V a given potential (note that $V = 0$ leads to Burgers equation), the moments can be shown to satisfy the infinite hierarchic system

$$\partial_s m_k(s, x) + \partial_x m_{k+1}(s, x) + k\partial_x V(s, x)m_{k-1}(s, x) = 0 \tag{48}$$

for $k = 0, 1, 2, ...$ with $m_{-1} = 0$ by convention. The q variable is eliminated as in the Hamilton-Jacobi equation and dimensionality then reduced. The moments still carry information on the multi-valued structure of the GO solution : let us for instance consider a phase-space solution with two branches $p_i(s, x)$ $i = 1, 2$. We recall that f represents a density of particles that moves according to the Hamiltonian dynamics. The simplest representation for f is given (see also (31)) by

$$f(s, x, q) = \sum_{i=1}^{2} \delta(q - p_i(s, x)),$$

i.e. we simply count the number of rays going through (s, x). It is also possible to transport a characteristic function bounded by the curves $p_i(s, x)$ (a technique inspired by the transport collapse method [22]) :

$$f(s, x, q) = H(p_2(s, x) - q) - H(p_1(s, x) - q) \tag{49}$$

where H is the Heavyside function and we suppose that $p_2 > p_1$. Then several remarkable simplifications occur. The first two moments satisfy

$$\begin{cases} m_0 = p_2 - p_1 \\ m_1 = \frac{1}{2}(p_2^2 - p_1^2) \end{cases} \tag{50}$$

which can be easily inverted point-wise. The bi-valued GO solution is easily recovered from the first two moments. The special form (49) also provides the closure formula

$$m_2 = \frac{m_1^2}{m_0} + \frac{1}{12}m_0^3$$

which enables the truncation of (48) at $k = 1$ and the computation of the first two moments. More on the numerical resolution of (48) can be found in [27]. A general closure procedure is also proposed for a finite number of branches in the spirit of the closure of Boltzmann moment equations [60].

The application of this method to the "real" GO problem turns out to be nontrivial [36] [74]. First notice that the paraxial model with the Hamiltonian function (3) does not allow the derivation of a similar moment system but the full 2-D Hamiltonian function (12) $H(X, P) = \frac{1}{2}(\|P\|^2 - \frac{1}{c^2(X)})$ has a form similar to (47) and obeys the same Hamiltonian dynamics (10). A kinetic equation similar to (29) can be derived in this 2-D setting :

$$f_s(s, X, Q) + \nabla_X H(X, Q) \cdot \nabla_X f(s, X, Q) - \nabla_P H(s, X, Q) \cdot \nabla_Q f(s, X, Q) = 0. \tag{51}$$

Setting $X = (x_1, x_2)$ and $Q = (q_1, q_2)$, we have a two parameter family of moments

$$m_{k,l}(s, X) = \int q_1^k q_2^l f(s, X, Q) dQ$$

which satisfy the 2-D extension to system (48)

$$\begin{aligned}
&\partial_s m_{k,l}(s, X) + \partial_{x_1} m_{k+1,l}(s, x) + \partial_{x_2} m_{k,l+1}(s, x) + \\
&k\, \partial_{x_1}(\frac{1}{c^2(X)}) m_{k-1,l}(s, X) + l\, \partial_{x_2}(\frac{1}{c^2(X)}) m_{k,l-1}(s, X) = 0
\end{aligned} \tag{52}$$

for all integers $k, l \geq 0$ and with the same convention $m_{k,-1} = m_{-1,l} = 0$. Assuming a finite number N of branches the density function is chosen in the form

$$f(s, X, Q) = \sum_{i=1}^{N} a_i(s, X) \delta(\|Q\| - \frac{1}{c^2(X)}) \delta(arg(Q) - \theta_i(s, x)).$$

This formula is similar to (31), a_i and θ_i represent respectively the amplitude and direction angle of the ith ray at position (s, X) . The Eikonal equation (8) forces the modulus of the ray vector P_i to be equal to $\frac{1}{c^2}$ and is allowed as an unknown only the angle θ_i this vector makes with a fixed given direction. The point-wise relation between the moments and the multi-phase Eulerian amplitudes and angles becomes the (non-linear) system

$$m_{k,l} = \sum_{i}^{N} a_i (\frac{1}{c^2})^{k+l} \cos^k \theta_i \sin^l \theta_i \tag{53}$$

The polar decomposition of the ray vector therefore reduces the problem with N phases including amplitudes computations to $2N$ variables instead of $3N$. In [74] the authors explain how, by carefully choosing $2N$ moments, it is possible to close system (52). Analytical and numerical inversion procedures are discussed for (53). A comprehensive numerical analysis of (52) is also done explaining the difficulties of this method. Numerical results for two phases are provided.

The moment method has also been applied to multi-phase calculation for the Schrödinger equation [51].

7   Dynamic surface extension (DSE)

It is difficult to decide whether the DSE method of John Steinhoff is Eulerian or Lagrangian. It is probably safe to say that it belongs to both families and even safer to describe it in a separate section .

The algorithm borrows its dynamics from ray tracing but uses a fixed grid for the representation of the front. Ultimately it can be understood as a (rather involved) interpolation method to sample as "uniformly" as possible the front. I simplify the presentation by considering, as in section 4, the curve $\{y(s, y_0)/y_0 \in D\}$ (D being an initial set of rays) that moves according to the Lagrangian equations (2). A fixed "Eulerian" grid is given and, at

fixed time s and for each grid point x_i ($i \in I$) the closest front point in term of a distance (the Euclidean distance is the simplest choice) is computed :

$$y_{0,i} = \mathrm{arginf}_{y_0 \in D} \| x_i - y(s, y_0) \| \tag{54}$$

The front at "time" $s + ds$ is then represented by the discrete set $\{y(s + ds, y_{0,i})/i \in I\}$. Actually, it necessary to compute and store the set of bicharacteristics $(y(s + ds, y_{0,i}), p(s + ds, y_{0,i}))_{i \in I}$. As the front moves, its closest grid point representation also changes and must be recomputed as in (54) but at time $s + ds$. This "closest point" projection step is the feature that distinguishes DSE from plain RT. At each "time" step (or possibly at every n^{th} time step) a new representation of the front is calculated. As the front is sampled on the grid, some interpolation method is of course needed to maintain a reasonable degree of accuracy in its reconstruction.

As the grid points are fixed and uniformly distributed (note that this is not a prerequisite of the method) the resolution of the front cannot get worse than the step of the grid itself. Multi-phase solutions naturally project on different families of points and interpolation between points projecting onto different branches may produce spurious results. Fronts merging, as in the case of a true focal point where all rays cross at same "time" s, is pathological : all grid points project on the same (single) front point and the phase-space information (the p variable) is lost. One could think of several ways to fix this problem but still this is an indication that the method can underresolve converging front behavior that occurs on a scale smaller than the grid step. The case of the cusped caustic is analyzed in [65] where a fix is proposed based on several modification of the distance used in the projection step (54).

One can look at DSE with a "level set" point of view. This method uses again a fixed Eulerian 2-D grid to compute the motion of a 1-D curve. The "closest point" front representation is clearly highly redundant. A "fast marching" band limitation is certainly recommended to keep the computational cost of DSE reasonable.

References

[1] R. Abgrall. Numerical Discretization of First Order Hamilton Jacobi Equations on Triangular Meshes. Comm. Pure Appl. Math. **49** (1996), no. 12, 1339–1373.

[2] R. Abgrall. Numerical approximation of boundary conditions for Hamilton Jacobi equations Siam J. Numer. Anal., in revision.

[3] R. Abgrall and S. Augoula High Resolution Schemes for First Order Hamilton Jacobi Equations on Triangular Meshes. J. Sci. Comput. **15** (2000), no. 2, 197–229;

[4] R. Abgrall and J.-D. Benamou. Big ray tracing and Eikonal solver on unstructured grids : Application to the computation of a multi-valued travel-time field in the marmousi model. Geophysics **64** (1999), 230–239.

[5] V. I. Arnol'd. *Mathematical methods of Classical Mechanics.* Springer-Verlag, 1978.

[6] V. I. Arnol'd. *Catastrophe theory.* Springer-Verlag, 1992.

[7] V. I. Arnol'd, S.M. Gusein-Zade, and A.N. Varchenko. *Singularities of Differential Maps.* Birkhauser, 1986.

[8] C.Bardos, G. Lebeau and M.Rausch. Sharp sufficient conditions for the observability, control and stabilization of waves from the boundary. SIAM J. Cont Optim. **30** (1992) 1024–1065.

[9] G. Barles. *Solutions de viscosité des équations de Hamilton-Jacobi.* Collection Math. Appliquées, Springer-Verlag, 1994.

[10] J.-D. Benamou. Eulerian Geometrical Optics. ESAIM proc., to appear (2002).

[11] J.-D. Benamou. Direct solution of multi-valued phase-space solutions for hamilton-jacobi equations. Comm. Pure Appl. Math. **52** (1999) 1443–1475.

[12] J.-D. Benamou. Equations "géométriques" pour les calcul d'amplitudes d'ondes haute fréquence. *preprint, http://www-rocq.inria.fr/˜benamou*, 1999.

[13] J.-D. Benamou and I. Solliec. An eulerian method for capturing caustics. J. Comput. Phys. 162 (2000), no. 1, 132–163.

[14] J.-D. Benamou, O. Lafitte, R. Sentis and I. Solliec. A geometric optics method for high frequency electromagnetic field computations near fold caustics - Part I. *preprint, http://www-rocq.inria.fr/˜benamou*, 2002.

[15] J.-D. Benamou, O. Lafitte, R. Sentis and I. Solliec. A geometric optics method for high frequency electromagnetic fields computations near fold caustics - Part II. *preprint, http://www-rocq.inria.fr/˜benamou*, 2002.

[16] J.-D. Benamou, F. Castella, T. Katsaounis and B. Perthame High frequency limit of the Helmholtz equation. Rev. Mat. Iberoamericana **18** (2002) 187–209.

[17] M. Berry. Rays, wavefronts and phase: a picture book of cusps. In H.K. Kuiken H. Blok, H.A. Fewerda, editor, *Huygens' Principle 1690-1990 : Theory and Applications.* Elsevier, 1992.

[18] G. Beylkin. Imaging of discontinuities in the inverse scattering problem by inversion of a causal generalized radon transform. Journal of Mathematical Physics **26** (1985) 99–108.

[19] N. Bleistein and S. H. Gray. An extension of the born inversion method to a depth dependent reference profile. Geophysical Prospecting **33** (1985) 999–1022.

[20] J. F. Bonnans and H. Zidani. Consistency of generalized finite difference schemes for the stochastic HJB equation. *INRIA tech. report*, RR 4162 .

[21] D. Bouche and F. Molinet. Asymptotic methods in electromagnetics. *Springer-Verlag*, 1994.

[22] Y. Brenier. Averaged multi-valued solutions for scalar conservation laws. Siam J. Numer. Anal. **21** (1984) 1013–1037.

[23] P. Bulant. Two-Point ray tracing in 3-D. Pure and Applied Geophysics **148** (1996) 421–446.

[24] P. Bulant and L. Klimes. Interpolation of ray-theory travel times withon rays. Geophysical Journal International **139** (1999) 273–282.

[25] F. Castella, B. Perthame and O. Runborg High frequency limit of the Helmholtz equation II : source on a general smooth manifold. *report DMA-00-34, http://www.dma.ens.fr/users/perthame*, 2001.

[26] S. Geoltrain and J. Brac. Can we image complex structures with first-arrival travel-time ? Geophysics **58** (1993) 564–575.

[27] Y. Brenier and L.Corrias. A kinetic formulation for multibranch entropy solutions of scalar conservation laws. Ann. Inst. H. Poincaré Anal. Non Linéaire **15** (1998), no. 2, 169–190.

[28] C.H. Chapman and C.J. Thomson An introduction to Maslov's asymptotic method. Geophys. J. R. astr. Soc. **83** (1983) 143–168.

[29] S. Osher, L.T. Cheng, M. Kang, H. Shim and Y.-H. Tsai. Geometric Optic in a Phase-Space Based Level Set and Eulerian Framework. *preprint, http://www.levelset.com/lss.html*.

[30] R. Courant and D. Hilbert. Methods of mathematical physics. Vol. II. Partial differential equations, Reprint of the 1962 original, A Wiley-Interscience Publication (1989).

[31] M.G. Crandall and P.L. Lions. Viscosity solutions of hamilton-jacobi equations. Trans. Amer. Math. Soc. **277** (1983) 1–42.

[32] M.G. Crandall and P.L. Lions. Two approximation solutions of hamilton-jacobi equations. Math. Comp. **43** (1984) 1–19.

[33] J.J. Duistermaat. Oscillatory integrals, lagrange immersions and unfolding of singularities. Comm. Pure Appl. Math. **27** (1974) 207–281.

[34] B. Engquist, E. Fatemi and S. Osher. Numerical resolution of the high frequency asymptotic expansion of the scalar wave equation. J. Comp. Physics **120** (1995) 145–155.

[35] J. B. Keller, D. W. McLaughlin and G. C. Papanicolaou *Surveys in applied mathematics.* Vol. 1, Plenum, New York, 1995;

[36] B. Engquist and O. Runborg. Multiphase computation in geometrical optics. J. Comput. Appl. Math. 74 (1996), no. 1-2, 175–192.

[37] B. Engquist, O. Runborg and A.-K. Tornberg. High Frequency Wave Propagation by the Segment Projection method. UCLA CAM Report 01-13, 2001.

[38] J. Steinhoff M. Fan and L. Wang. A new eulerian method for the computation of propagating short acoustic and electromagnetic pulses. J. Comp. Physics **57** (2000), no. 2, 683–706.

[39] M. V. Fedoryuk. *Partial Differential Equations (Chap. 1).* Springer-Verlag, 1988.

[40] W.H. Fleming and W.M McEneaney. A Max-Plus based algorithm for an HJB equation of nonlinear filtering. SIAM J. Control Optim. **38** (2000) 683–710.

[41] S. Fomel and J.A. Sethian. Fast Phase-Space Computation of Multiple Arrival. Proc. Natl. Acad. Sci. USA 99 (2002), no. 11, 7329–7334.

[42] I.M. Gelfand and S.V Fomin. *Calculus of Variation.* Prentice-Hall, 1963.

[43] P. Gérard and É. Leichtnam. Ergodic properties of eigenfunctions for the Dirichlet problem *Duke Math. J.* 2:559–607, 1993.

[44] E. Godlewski and P.A. Raviart. Numerical approximation of hyperbolic systems of conservation laws. *Applied Mathematical Sciences*, 118. Springer-Verlag, New York, 1996.

[45] F. Golse, O. Lafitte and R. Sentis. Sur la simulation numérique de la propagation laser. *Rapport CEA*, 1999.

[46] S. Gray and W. May Kirchhoff migration using eikonal equation travel-times Geophysics **59** (1994) 810–817.

[47] E. Hairer, C. Lubich and G. Wanner, *Geometric numerical integration* Springer, Berlin, 2002.

[48] P. Hoch and M. Rascle. Hamilton-Jacobi Equations on a Manifold and Applications to Grid Generation or Refinement. *Preprint, http://www-math.unice.fr/~rascle/.*

[49] S. Izumiya. The theory of legendrian unfoldings and first order differential equations. Proc. Royal Soc. Edinburgh **123** (1993) 517–532.

[50] Izumiya, S.; Kossioris, G. T.; Makrakis, G. N. Multi-Valued solutions to the Eikonal equation in stratified media. Quart. Appl. Math. 59 (2001), no. 2, 365–390

[51] S. Jin and X. Li. MultiPhase computations of the semiclassical limit of the Schrödinger equation and related problems: whitam vs Wigner. *Preprint, http://www.math.wisc.edu/~jin.*

[52] G-S. Jiang and D. Peng Weighted ENO schemes for hamilton-jacobi equations. SIAM J. Sci. Comput. **21** (2000) 2126–2143.

[53] M. Kang, B. Merryman, S.J. Osher, D. Peng and H. Zhao. A PDE based fast level set method. J. Comput. Phys., **155** (1999) 410–438.

[54] Katsaounis, T.; Kossioris, G. T.; Makrakis, G. N. Computation of high frequency fields near caustics. Math. Models Methods Appl. Sci. **11** (2001), no. 2, 199–228.

[55] G. T Kossioris, C.H. Makridakis, P. E. Souganidis. Finite Volume Schemes for Hamilton-Jacobi equations. Numer. Math. 83 (1999), no. 3, 427–442.

[56] J.B. Keller. A geometrical theory of diffraction. In *Calculus of variations and its applications Vol, 8.* McGraw-Hill, New-York, 1958.

[57] A. Kurganov and E. Tadmor. NEw High-Resolution Semi-Discrete Central Schemes for hamilton-jacobi equations. J. Comput. Phys. **160** (2000) 720–742.

[58] G. Lambare, P. Lucio, and A. Hanyga. Two dimensional multi-valued travel-time and amplitude maps by uniform sampling of a ray field. Geophys. J. Int **125** (1996) 584–598.

[59] Piserchia P.F., Virieux J., Rodrigues D., Gaffet S., Talandier J. A hybrid numerical Modeling of T-Waves propagation: application to the Midplate experiment Geophys. J. Int. **133** no 3 (1998) 789–800.

[60] C.D. Levermore and W. J. Morokoff The Gaussian moment closure for gas dynamics. SIAM J. Appl. Math. **59** (1999) 72–96.

[61] P. L. Lions and T. Paul. Sur les mesures de Wigner. Rev. Mat. Iberoamericana **9** (1993) 553–618.

[62] P.S. Lucio, G. Lambare and A. Hayga. 3D Multi-Valued travel time and amplitude maps. Pure and Applied Geophysics **148** (1996) 449–476.

[63] D. Ludwig. Uniform asymptotic expansions at a caustic. Comm. Pure Appl. Math. **19** (1966) 215–250.

[64] P. A. Markowitch, N. J. Mauser and C. Sparber. Multi-Valued Geometrical Optics: Wigner Functions versus WKB-Methods. *to appear in Asymptotic Analysis*, 2002.

[65] B. Merryman S. Ruuth and S.J. Osher. A fixed grid method for capturing the motion of self-intersecting interfaces and related pdes. J. Comput. Phys. 163 (2000), no. 1, 1–21.

[66] T.J. Moser and J. Pajchel Recursive seismic ray modelling : applications in inversion and VSP. Geophysical Prospecting **45** (1997) 885–908.

[67] G. Namah and J.-M. Roquejoffre. Remarks on the long time behaviour of the solutions of Hamilton-Jacobi equations. Comm. Partial Differential Equations **24** (1999) 883–893.

[68] S. Osher and J.A. Sethian. Fronts Propagating with Curvature-Dependent Speed: Algorithms Based on Hamilton–Jacobi Formulations. Journal of Computational Physics **79** (1988) 12–49.

[69] S. J. Osher and C.W. Shu. High-order essentially nonoscillatory schemes for hamilton-jacobi equations. SIAM J. Numer. Anal. **83** (1989) 32–78.

[70] S. J. Osher and L. Rudin Rapid convergence of approximate solution to shape form shading problem. *Never Published - Not available.*

[71] J.L. Qian and W. Symes. An adaptive finite difference method for travel-time and amplitudes. Geophysics **67** (2002) 167–176.

[72] J.L. Qian and W. Symes. Finite-difference quasi-P travel-times for anisotropic media. Geophysics **67** (2002) 147-155.

[73] E. Rouy and A. Tourin. A viscosity solutions approach to shape-from-shading. SIAM J. Numer. Anal. **3** (1992) 867–884.

[74] O. Runborg. Some new results in multiphase geometrical optics. M2AN Math. Model. Numer. Anal. 34 (2000), no. 6, 1203–1231.

[75] J.A. Sethian. A Fast Marching Level Set Method for Monotonically Advancing Fronts. *Proc. Nat. Acad. Sci.* 93:1591–1595, 1996.

[76] J.A. Sethian. *Level Set Methods and Fast Marching Methods Evolving Interfaces in Computational Geometry, Fluid Mechanics, Computer Vision, and Materials Science.* J.A. Sethian, Cambridge University Press, 1999.

[77] P. E. Souganidis. Approximation schemes for hamilton-jacobi equations. J. Differential Equations **59** (1985) 1–43.

[78] W. Symes. A slowness matching algorithm for multiple travel-times. *this issue*, 2002.

[79] W. Symes, R. Versteeg, A. Sei, and Q. H. Tran. Kirchhoff simulation migration and inversion using finite-difference travel-times and amplitudes. *TRIP tech. Report, Rice U.*, 1994.

[80] J. Van Trier and W. W. Symes. Upwind finite-difference calculation of travel-times. Geophysics **56** (1991) 812–821.

[81] J. Vidale. Finite-difference calculation of travel-times Bull. Seis. Soc. Am. **78** (1988) 2062–2076.

[82] V. Vinje, E. Iversen, and H. Gjoystdal. Travel-Time and amplitude estimation using wavefront construction. Geophysics **58** (1993) 1157–1166.

[83] V. Vinje, E. Iversen, H. Gjoystdal adn K. Astebol. Estimation of multi-valued arrivals in 3-D models using using wavefront construction (Part I and II). Geophysical Prospecting **44** (1996) 819–858.

[84] L.C. Young. *Lecture on the Calculus of Variation and Optimal Control Theory*. W. B. Saunders Co., Philadelphia-London-Toronto, Ont. , 1969.